Trends in Inversion Barriers IV. The Group 15 Analogous of Pyrrole

Silke Pelzer, Karin Wichmann, Ralf Wesendrup, and Peter Schwerdtfeger*

Department of Chemistry, University of Auckland, Private Bag 92019, Auckland, New Zealand

Received: February 6, 2002; In Final Form: March 19, 2002

The inversion process of pyrrole, phosphole, arsole, stibole, and bismole is analyzed in detail by using ab initio and density functional techniques. The results are compared with the corresponding divinyl and diethyl compounds, $HM(C_2H_3)_2$ and $HM(C_2H_5)_2$, respectively (M = N, P, As, Sb, and Bi). The inversion barrier increases down the Group 15 elements and from the cyclic, via the divinyl to the diethyl compounds. The inversion process can be rationalized in terms of a second-order Jahn−Teller distortion using HOMO/LUMO energy differences. B3LYP calculations predict that fluorination of the pyrrole ring leads to nonplanar structures of both the tetra- and pentafluoropyrrole.

1. Introduction

Since Dennison and Hardy produced the first infrared spectrum of ammonia, showing inversion doubling as early as 1932, it has been accepted that NH_3 adopts a dynamic gas-phase structure.[1] This is due to quantum tunneling of the three hydrogen atoms through an estimated inversion barrier of ca. 24.2 kJ mol^{-1}. In general, the inversion barrier is low for amines NR_3 with electropositive ligands R. In the case of the doubly unsaturated cyclic derivative pyrrole, HNC_4H_4, the nitrogen atom has a planar environment. Here, the "hypothetical inversion barrier" is so small that nitrogen becomes part of a 6π aromatic ring system as shown in Figure 1. In contrast, the closely related singly unsaturated 2,5-dihydropyrrole adopts a nonplanar structure of C_s symmetry and Dommen et al. have recently studied the ring puckering motion.[2]

The classical inversion process of the pyramidal pnicogen hydrides and halides, MX_3 (M any Group 15 element), connects two degenerate minima of C_{3v}-symmetry through a trigonal-planar transition state of D_{3h}-symmetry, where the M lone pair orbital is purely of p-character. For the hydrides, the calculated inversion barriers increase significantly from NH_3 down the group 15 to BiH_3.[3] For PH_3, most calculations predict an inversion barrier between 140 and 150 kJ mol^{-1}.[4,5] Thus, it is not surprising that the ring system of the unknown compound phosphole, HPC_4H_4 is predicted to be nonplanar (Figure 1) and X-ray structures of substituted phospholes show indeed a pyramidal geometry about the phosphorus atom.[6] The electron pair at the phosphorus center participates little in π-conjugation with the ring moiety, which reduces the aromatic character as compared to pyrrole. Although the experimental barrier of inversion for phosphole is not known, a rather low value was predicted already 30 years ago due to partial π-conjugation in the planar transition state.[7] This is in line with the fact that phosphole derivatives cannot be obtained as single enantiomers due to rapid racemization about the phosphorus atom in contrast to some noncyclic phosphine compounds.[8] Nyulászi has calculated an inversion barrier of 90.1 kJ mol^{-1} for phosphole at the 6-311G** CCD (coupled cluster with doubles only) level of theory which is just about half the value obtained for PH_3 at the same level.[9] Delaere et al. came to very similar conclusions in a recent B3LYP study and found an inversion barrier of 72 kJ mol^{-1} for phosphole as compared to 139 kJ mol^{-1} for PH_3.[10] Electropositive ligands on the phosphorus center or π-acceptor substituents at various positions of the ring system can reduce the inversion barrier of phosphole significantly.[9,10] Interestingly, the isoelectronic compound pentaphosphole, P_5H is predicted to have a planar minimum structure as a result of aromaticity and electronegativity effects.[11]

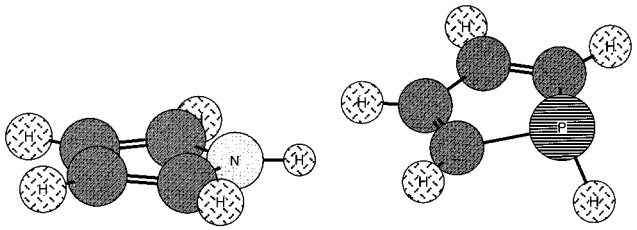

Figure 1. Optimized MP2 structures of pyrrole and phosphole.

In an earlier paper[5] in this series on inversion mechanisms, we pointed out that for the pnicogen fluorides PF_3, AsF_3, SbF_3, and BiF_3 the trigonal planar inversion transition state breaks symmetry to adopt a T-shaped C_{2v}-structure[12] due to a second-order Jahn−Teller distortion thus following a *nonclassical* edge inversion. In contrast to the corresponding hydrides, the inversion barrier *decreases* from NF_3 down the group to BiF_3 with NF_3 showing the highest inversion barrier of 400 kJ mol^{-1}. Fluorine substitution on the pyrrole ring system should therefore also increase the inversion barrier and might eventually lead to a nonplanar minimum structure like phosphole.

There have been a number of theoretical studies performed on unsaturated 5-ring systems, usually dealing with their degree of aromaticity,[9−11,13] their reactions or other molecular properties.[14] However, with the sole exception of phosphole their inversion barriers have not yet been studied. In the following, we present a comparative study of the inversion barriers of pyrrole, phosphole,[6] arsole, stibole, and bismole[15] by using ab initio and density functional based methods. These are compared with the corresponding divinyl and diethyl derivatives (see Figures 1 and 2) to allow for the discussion of the influence of ring π-conjugation and aromaticity to inversion barriers. The

10.1021/jp0203494 CCC: $22.00
Published on Web 06/12/2002

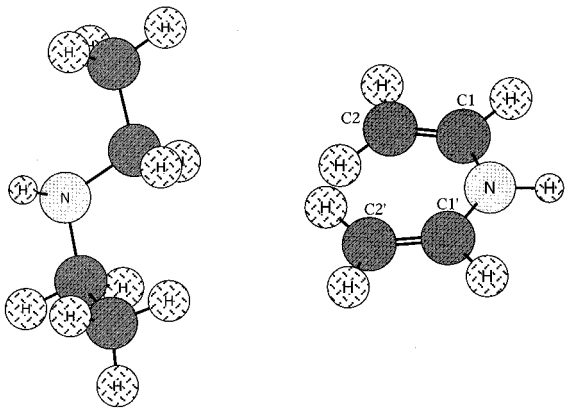

Figure 2. Optimized MP2 structures of diethyl and divinylamine.

effect of fluorination upon the geometry will also be discussed by studying selected fluorinated derivatives. We also reinvestigate the inversion barriers of NH_3 and PH_3 using Dunning's systematic correlation consistent basis sets.[16]

2. Computational Methods

All geometry optimizations and subsequent frequency analyses were carried out with the Gaussian98 program package.[17] The compounds HMC_4H_4, $HM(C_2H_3)_2$, and $HM(C_2H_5)_2$ (M = N, P, As, Sb, and Bi) were optimized at the Hartree−Fock (HF), second-order many-body perturbation theory (MP2) and density functional level (DFT); the latter using the hybrid ansatz of Becke[18] for the exchange functional together with the nonlocal ansatz of Lee, Yang, and Parr[19] for the correlation functional (B3LYP) as implemented in Gaussian98. The fluorinated derivatives of the cyclic compounds were only treated at the B3LYP level. Great care was taken to find the correct first-order saddle points. All determined transition states exhibit only one imaginary frequency with the corresponding Cartesian displacements mainly describing the inversion about the pnicogen atom. For carbon, nitrogen, fluorine, and phosphorus we used Dunning's correlation consistent triple-ζ-(cc-PVTZ) basis set without the f-functions.[16] For hydrogen, we applied the cc-PVTZ basis set without the d-function and the most diffuse p-function. Scalar relativistic multielectron adjusted Stuttgart pseudopotentials and corresponding valence basis sets were used for arsenic, antimony, and bismuth.[20] The basis sets were altered by decontracting the lowest s- and p-functions and adding soft s- and p-functions with exponent 0.03. Finally, two d-functions were added to all three sets with the following exponents: As 0.129 and 0.434; Sb 0.088 and 0.277; Bi 0.229 and 0.690.

In a previous paper on MX_3 systems (M group 15 element and X any ligand), we showed that the MP2 method yields reasonable results for the classical inversion process through a trigonal planar transition state when compared to experiment or a more expensive coupled cluster treatment.[3] To establish the relative accuracy of the B3LYP method for inversion barriers, we also present a systematic study of the inversion of NH_3 and PH_3 using the series of Dunning's augmented correlation consistent aug-cc-pVnZ basis sets (n = D, T, Q, Qi)[16] at B3LYP and the HF, MP2, and CCSD(T) level of theory.

3. Results and Discussion

A. NH_3 and PH_3. Tables 1 and 2 list the geometries, inversion barriers and harmonic frequencies at various levels of theory for the critical points of the inversion process of NH_3 and PH_3. Our CCSD(T) geometry using the quadruple-ζ basis set agrees with an earlier value of Halkier and Taylor,[21] and all our correlated results are in satisfactory agreement for geometric parameters. Figure 3 shows that for NH_3 the barrier converges relatively fast with increasing size of the basis set, as found before by Császár et al.[22] Compared to the more accurate CCSD(T) results, the inversion barrier is underestimated by the other methods by a few kJ mol^{-1}. Figure 3 also suggests that the CCSD(T) basis set limit for NH_3 lies between 21 and 22 kJ mol^{-1}, which is 2 kJ mol^{-1} lower than the experimentally estimated value of 24.2 kJ mol^{-1} found in most textbooks.[23] However, our value is in very good agreement with a recent study by Klopper et al. who derived a final value of 1777 ± 12 cm^{-1} (21.3 kJ mol^{-1}) for the inversion barrier after a careful investigation of relativistic and correlation effects.[24] One might, therefore, suspect that the originally derived experimental value of 24.2 kJ mol^{-1} is inaccurate. This value bases on a one-dimensional fit of the double-minimum potential to experimental frequencies and neglects coupling effects from the full NH_3 hypersurface.[23,25] A more recent multidimensional treatment derived from experimental rovibrational spectra by Spirko and

TABLE 1: Optimized Parameters for NH_3 Using the Aug-cc-pVnZ (n = D, T, Q, Qi) Dunning Basis Sets at the HF, MP2, CCSD(T), and B3LYP Level of Theory[a]

n		r_e	α_e	r_T	ΔE_a	$\nu_1(A_1)$	$\nu_2(A_1)$	$\nu_3(E)$	$\nu_4(E)$
D	HF	1.004	107.57	0.990	21.44	3680	1106	3812	1767
	MP2	1.020	106.31	1.003	21.95	3484	1047	3639	1651
	CCSD(T)	1.023	105.98	1.005	24.13	3431	1072	3569	1653
	B3LYP	1.019	106.77	1.002	19.64	3457	1021	3586	1640
T	HF	0.999	108.12	0.985	20.20	3688	1096	3813	1787
	MP2	1.010	106.83	0.994	19.78	3533	1035	3663	1669
	CCSD(T)	1.012	106.76	0.995	21.67	3498	1049	3609	1672
	B3LYP	1.013	107.23	0.997	19.22	3468	1026	3587	1664
Q	HF	0.998	108.15	0.985	20.02	3690	1095	3815	1787
	MP2	1.008	107.22	0.993	19.85	3529	1022	3679	1673
	CCSD(T)	1.011	106.72	0.994	21.74	-	-	-	-
	B3LYP	1.012	107.27	0.997	19.02	3469	1024	3588	1664
Qi	HF	0.998	108.16	0.984	20.00	3691	1095	3816	1787
	MP2	1.007	107.14	0.992	19.72	3527	1028	3678	1677
	B3LYP	1.012	107.28	0.997	19.00	3473	1023	3593	1664
Exp.					24.2	3337	950	3414	1628

[a] Equilibrium bond distance r_e and distance for the D_{3h} structure r_T in Å, H−N−H bond angle α_e in degrees, inversion barrier ΔE_a (not corrected for zero-point vibration) in kJ mol^{-1} and harmonic frequencies ν in cm^{-1}. Experimental frequencies are from ref 26.

TABLE 2: Optimized Parameters for PH_3 Using the Aug-cc-pVnZ (n = D, T, Q, Qi) Dunning Basis Sets at the HF, MP2, and B3LYP Level of Theory[a]

n		r_e	α_e	r_T	ΔE_a	$\nu_1(A_1)$	$\nu_2(A_1)$	$\nu_3(E)$	$\nu_4(E)$
D	HF	1.418	95.53	1.382	149.02	2525	1090	2528	1224
	MP2	1.425	93.70	1.388	138.99	2463	1015	2481	1160
	CCSD(T)	1.433	93.51	1.393	142.98	2393	1014	2408	1142
	B3LYP	1.434	93.37	1.394	140.98	2365	1002	2379	1119
T	HF	1.408	95.60	1.373	148.12	2532	1096	2532	1232
	MP2	1.407	92.97	1.372	141.17	2484	1034	2496	1184
	CCSD(T)	1.414	92.85	1.377	144.78	2420	1034	2427	1166
	B3LYP	1.421	93.50	1.383	139.03	2386	1014	2394	1137
Q	HF	1.405	95.64	1.371	148.58	2535	1100	2532	1234
	MP2	1.403	93.54	1.368	135.63	2471	1017	2483	1168
	B3LYP	1.418	93.59	1.380	139.33	2389	1017	2395	1139
Qi	HF	1.404	95.64	1.370	149.24	2538	1102	2535	1235
	MP2	1.401	93.53	1.367	135.69	2488	1017	2497	1170
	B3LYP	1.417	93.60	1.379	139.95	2391	1017	2398	1139
Exp.						2327	991	2421	1121

[a] Equilibrium bond distance r_e and distance for the D_{3h} structure r_T in Å, H−N−H bond angle α_e in degrees, inversion barrier ΔE_a (not corrected for zero-point vibration) in kJ mol^{-1} and harmonic frequencies ν in cm^{-1}. Experimental frequencies are from ref 28.

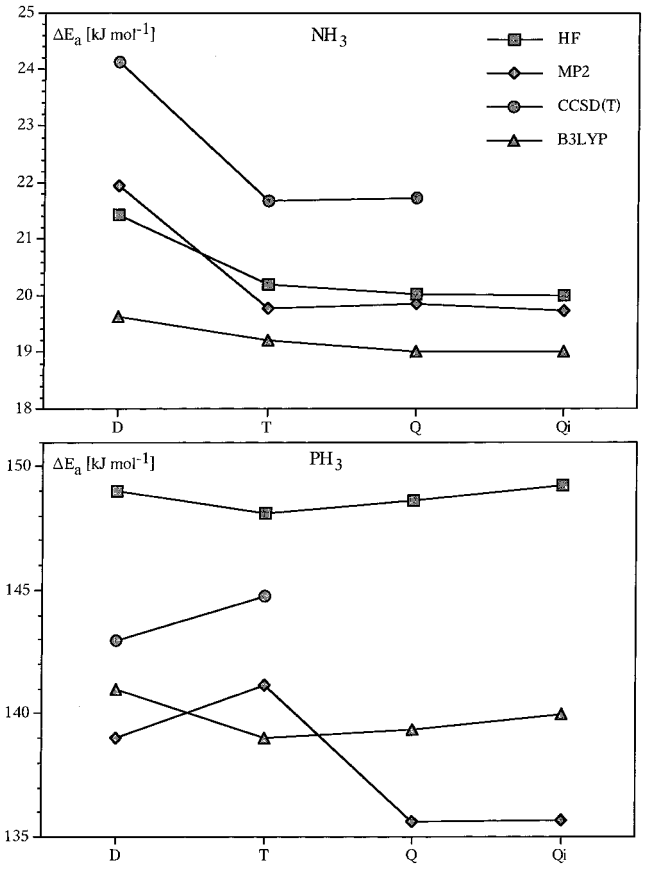

Figure 3. Inversion barriers ΔE_a for NH_3 and PH_3 as a function of the basis set size using Dunning's aug-cc-pVnZ basis sets (n = D, T, Q, and Qi).

Kraemer[26] (after correcting for zero-point vibrational effects from complementary modes)[22] and Maessen et al.[27] yields barriers around 1800 cm^{-1} (ca. 21 kJ mol^{-1}), which agree much better with our results. The experimental ν_2 inversion mode (0→1 transition) for NH_3 is 950 cm^{-1}, averaged over both inversion-splitting states.[26] Our corresponding harmonic frequencies given in Table 1 lie all above 1000 cm^{-1}, which is in line with the known significant anharmonicity effects of the NH_3 potential function.

For PH_3, the situation is less straightforward because the convergence of the barrier height with increasing size of the basis set is not smooth, see Figure 3. Coupled cluster calculations beyond aug-cc-pVTZ are currently beyond our computational resources, but the effect of an increased basis set can be estimated from the MP2 results. If we correct our aug-cc-pVTZ CCSD(T) value by using the MP2 results, we obtain an estimate of 139 kJ mol^{-1} for the inversion barrier of PH_3 as a benchmark. This is slightly lower than earlier predictions.[4] Interestingly, this value is in excellent agreement with the B3LYP results where the inversion barrier is almost independent of the basis set used. As for NH_3 the B3LYP geometries agree well with the CCSD(T) results. In contrast to NH_3, the calculated harmonic frequencies come very close to the experimental values.[28] We therefore conclude that both the MP2 and the B3LYP procedures give reasonably accurate results for inversion barriers and should be ideally suited for the larger Group 15 organic compounds.

B. Group 15 Organic Compounds. *Structures.* The more important structural data for all minima and inversion transition states of HMC_4H_4, $HM(C_2H_3)_2$ and $HM(C_2H_5)_2$ (M = N, P, As, Sb and Bi) are listed in Tables 3 and 4 according to the definition in Figure 2. Much to our surprise, experimental gas phase or crystal structural data seem only available for pyrrole[29] and diethyl-amine.[30] Some crystal structures for substituted phospholes, arsoles and stiboles are known and the divinyl compounds $HM(C_2H_3)_2$ have been synthesized for M = P, As and Sb, but only been characterized by NMR, MS and − for As − IR spectroscopy.[31] In all cases, the agreement between experimental data and our calculations is very good. For example, the CMH angle, calculated at the B3LYP/MP2 level compares to the experimental values set in parentheses: 125.1°/124.9° (125.1°) for pyrrole, 109.4°/108.8° (107.9°) for diethyl-amine and 90.6°/90.1° (90.7°) for phosphole.[32] The increasing M−C bond length with increasing nuclear charge of the heteroatom M corresponds to a decreasing CMC bond angle in agreement with the findings of Baldridge and Gordon.[13a] This holds true for all investigated systems including the ethyl and vinyl derivatives and the inversion transition structures. Only for the global minima of pyrrole and divinylamine, we find a trigonal planar arrangement in the C_2NH moiety. For divinyl-amine a fully symmetric C_{2v} structure is obtained at the B3LYP level. However, in the optimized MP2 geometry, shown in Figure 2, a small distortion occurs which is best seen in the C=C−N−C torsion angle of 8.8°. A similar situation is found for the corresponding planar structure of divinyl bismine, which represents a first-order saddle point. Again, the C_{2v} symmetry at B3LYP level is reduced to C_2 at the MP2 level. Apart from these minor differences, the symmetry of the stationary points is the same for both methods. In particular, the inversion

TABLE 3: Selected Molecular Structure Parameters (in Å and degrees) for the Minimum Structures of HMC_4H_4, $HM(C_2H_3)_2$, and $HM(C_2H_5)_2$ (M = N, P, As, Sb, and Bi) at the MP2 and B3LYP Level of Theory[a]

	method	r_{M-C1}	r_{M-H}	r_{C1-C2}	$r_{C2-C2'}$	$\alpha_{C1-M-C1'}$	$360-\Sigma\alpha$
				HMC_4H_4			
N	MP2	1.372	1.011	1.384	1.419	110.2	0
	B3LYP	1.372	1.008	1.373	1.421	109.8	0
P	MP2	1.803	1.425	1.363	1.449	90.6	66.7
	B3LYP	1.813	1.424	1.349	1.455	90.1	67.6
As	MP2	1.934	1.531	1.356	1.456	86.0	81.2
	B3LYP	1.946	1.532	1.342	1.462	85.6	80.6
Sb	MP2	2.139	1.727	1.354	1.463	80.5	90.3
	B3LYP	2.149	1.724	1.341	1.467	80.2	89.4
Bi	MP2	2.238	1.828	1.352	1.465	78.0	96.8
	B3LYP	2.242	1.817	1.338	1.470	77.9	94.4
				$HM(C_2H_3)_2$			
N	MP2	1.386	1.009	1.343		130.2	0
	B3LYP	1.385	1.007	1.336		131.4	0
P	MP2	1.829	1.427	1.338		99.9	66.3
	B3LYP	1.834	1.427	1.328		101.9	64.6
As	MP2	1.947	1.533	1.337		96.9	73.4
	B3LYP	1.959	1.534	1.326		98.8	71.6
Sb	MP2	2.147	1.729	1.338		94.0	78.4
	B3LYP	2.158	1.727	1.327		96.0	76.6
Bi	MP2	2.245	1.831	1.338		92.0	82.1
	B3LYP	2.251	1.820	1.326		94.6	79.1
				$HM(C_2H_5)_2$			
N	MP2	1.462	1.021	1.522		114.1	28.3
	B3LYP	1.462	1.018	1.526		115.6	25.6
P	MP2	1.860	1.430	1.525		101.9	64.5
	B3LYP	1.873	1.429	1.527		102.6	63.2
As	MP2	1.979	1.535	1.523		99.3	70.9
	B3LYP	1.996	1.536	1.525		100.0	69.3
Sb	MP2	2.180	1.733	1.524		96.4	76.8
	B3LYP	2.196	1.728	1.526		97.1	75.0
Bi	MP2	2.275	1.832	1.523		95.1	80.8
	B3LYP	2.286	1.820	1.523		95.9	77.6

[a] For structures of low symmetry averaged r_{M-C1} and r_{C1-C2} bond distances are used. See Figure 2 for parameter definitions.

TABLE 4: Selected Molecular Structure Parameters (in Å and degrees) for the Inversion Transition State Structures of HMC_4H_4, $HM(C_2H_3)_2$, and $HM(C_2H_5)_2$ (M = N, P, As, Sb, and Bi) at the MP2 and B3LYP Level of Theory[a]

	method	r_{M-C1}	r_{M-H}	r_{C1-C2}	$r_{C2-C2'}$	$\alpha_{C1-M-C1'}$
			HMC_4H_4			
N	MP2	1.372	1.011	1.384	1.419	110.2
	B3LYP	1.372	1.008	1.373	1.421	109.8
P	MP2	1.718	1.400	1.400	1.413	99.2
	B3LYP	1.724	1.395	1.386	1.417	98.6
As	MP2	1.829	1.486	1.394	1.415	95.0
	B3LYP	1.840	1.482	1.375	1.424	94.2
Sb	MP2	2.034	1.672	1.388	1.420	88.0
	B3LYP	2.049	1.664	1.366	1.434	87.0
Bi	MP2	2.124	1.762	1.383	1.419	85.4
	B3LYP	2.137	1.743	1.357	1.437	84.3
			$HM(C_2H_3)_2$			
N	MP2	1.386	1.009	1.343		130.2
	B3LYP	1.385	1.007	1.336		131.4
P	MP2	1.756	1.393	1.347		126.1
	B3LYP	1.759	1.389	1.338		127.4
As	MP2	1.867	1.481	1.343		125.3
	B3LYP	1.874	1.479	1.334		126.8
Sb	MP2	2.078	1.669	1.341		123.2
	B3LYP	2.085	1.665	1.330		125.7
Bi	MP2	2.167	1.753	1.337		121.9
	B3LYP	2.177	1.749	1.326		127.8
			$HM(C_2H_5)_2$			
N	MP2	1.438	1.007	1.523		121.2
	B3LYP	1.440	1.005	1.527		122.2
P	MP2	1.832	1.396	1.526		122.0
	B3LYP	1.842	1.392	1.529		123.4
As	MP2	1.944	1.486	1.521		121.1
	B3LYP	1.963	1.485	1.523		123.2
Sb	MP2	2.154	1.677	1.520		122.2
	B3LYP	2.174	1.673	1.520		123.9
Bi	MP2	2.251	1.770	1.513		124.3
	B3LYP	2.276	1.765	1.511		126.6

[a] For structures of low symmetry averaged r_{M-C1} and r_{C1-C2} bond distances are used. See Figure 2 for parameter definitions.

transition states of all 5-ring systems are of C_{2v} symmetry and exhibit a perfectly planar arrangement. They are characterized by only one imaginary frequency in the harmonic frequency analysis that describes the out of plane motion of the hydrogen at the pnicogen atom.

The tendency to nonplanarity around the C_2MH unit can be expressed by the angle

$$\beta = 360° - \sum_{i=1}^{3} \alpha_i = 360° - (\alpha_{CMC'} + \alpha_{CMH} + \alpha_{HMC'}) \quad (1)$$

where a planar C_2MH arrangement corresponds to $\beta = 0°$.[4] The angle β systematically increases with the nuclear charge of element M (Table 3) for the cyclic, the divinyl, and the diethyl compounds, with only minor differences between MP2 and B3LYP. This increase in β is fully in line with the behavior of the group 15 hydrides and can be expected for classical inversion processes.[3,8,33] The planar C_2MH inversion structures possess shorter M−C and M−H bonds, as compared to the minimum nonplanar structures, in agreement with the fact that the group 15 element M changes formally from planar sp^2 to nonplanar sp^3 hybridization.

The C^1-C^2 bond distances (defined in Figure 2) remain almost constant throughout one series of group 15 compounds with the expected order r_{C-C}(vinyl) < r_{C-C}(5-ring) < r_{C-C}(alkyl). Interestingly, for the cyclic compounds the C^1-C^2 distances increase from the nonplanar to the planar inversion structure, whereas the $C^2-C^{2'}$ distances decrease. This observation has been made earlier in the inversion of phospholes[9,10] and was interpreted as an indication for the aromatic character of the planar transition state. A more quantitative measure for aromaticity is the Julg index J,[34] which defines the degree of aromaticity by the deviations of n individual C−C bond lengths r_i from the average C−C bond length r

$$J = 1 - (225/n) \cdot \sum_i \left(\frac{1 - r_i}{r}\right)^2$$

The Julg indices for the minima and planar transition states are shown in Figure 4 for pyrrole, phosphole, arsole, stibole, and bismole. In agreement with refs 10 and 13e, B3LYP yields lower Julg indices (or a more pronounced bond alternation) than MP2, but the qualitative features are the same for both methods. The planar transitions states are distinctly more aromatic than their corresponding bent minima with the maximum degree of aromaticity found for planar phosphole.[9] The aromatic character of the rings decreases from P toward the heavier homologues, more so for the minimum structures than for the planar transition states.

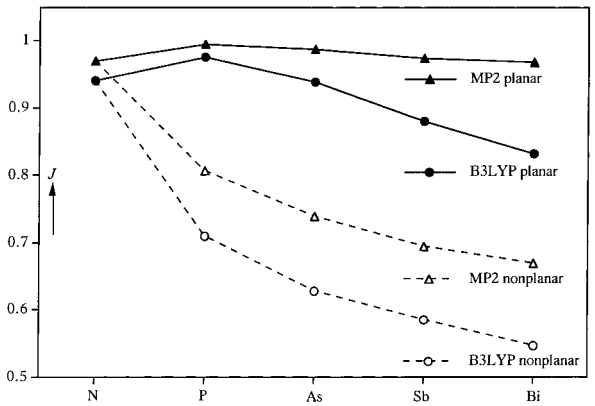

Figure 4. Julg index J for the (nonplanar) minimum and (planar) transition state ring structures of HMC_4H_4 at the MP2 and B3LYP level of theory. See text for definitions.

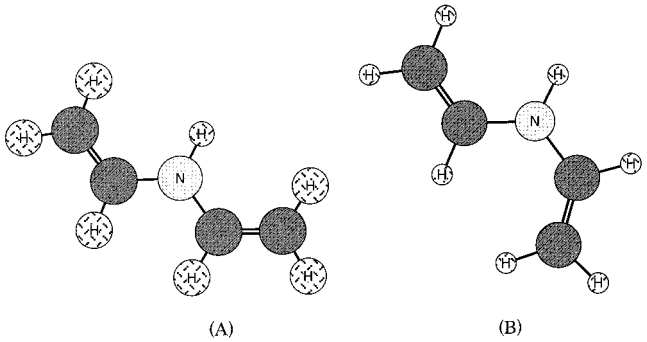

Figure 5. Optimized MP2 structures of two of the rotamers of divinylamine.

In addition to the C_{2v} structure shown in Figure 1, where both carbon chains are anti to the M−H bond in a ring like fashion, we also investigated the other two possible rotamers shown in Figure 5 for all Group 15 compounds. One rotamer is of C_{2v} symmetry and both vinyl groups are syn to the M−H bond, the other rotamer, containing one syn and one anti vinyl group is of C_s symmetry. The calculated energy differences between the three rotamers are listed in Table 5. Only for divinylamine we find the all-syn C_{2v} structure to be the global minimum. This rotamer is by 4−5 kJ mol^{-1} slightly more stable than the C_s structure and almost 10 kJ mol^{-1} lower in energy

TABLE 5: Energy Differences ΔE in kJ mol^{-1} of the Three Rotamers for the Inversion Transition State of $HM(C_2H_3)_2$ (M = N, P, As, Sb, and Bi)

	method	anti C_{2v}	syn C_{2v}	C_s
N	MP2	8.9	0	4.0
	B3LYP	12.2	0	5.2
P	MP2	0.0	6.1	5.0
	B3LYP	0.0	3.5	3.3
As	MP2	0.0	4.7	4.1
	B3LYP	0.0	2.1	2.3
Sb	MP2	0.0	3.4	3.0
	B3LYP	0.0	1.8	1.7
Bi	MP2	0.0	0.4	2.2
	B3LYP	0.0	0.8	0.9

TABLE 6: Calculated Inversions Barriers ΔE_a in kJ mol^{-1} for HMC_4H_4, $HM(C_2H_3)_2$, and $HM(C_2H_5)_2$ (M = N, P, As, Sb, and Bi)

	HF	MP2	B3LYP
		HMC_4H_4	
N	0.0	0.0	0.0
P	106.2	60.4	76.2
As	158.2	110.8	127.8
Sb	210.7	154.6	169.9
Bi	280.9	218.7	225.9
		$HM(C_2H_3)_2$	
N	0.0	0.0	0.0
P	146.6	119.6	106.4
As	187.9	162.6	155.9
Sb	223.3	194.5	187.9
Bi	292.5	255.8	242.4
		$HM(C_2H_5)_2$	
N	21.9	22.2	18.0
P	166.5	148.4	144.5
As	192.4	181.9	180.8
Sb	209.2	195.2	193.6
Bi	266.6	253.1	240.5

than the ring like C_{2v} form. For the other pnicogen atoms the ring like structure appears to be the global minimum. The energy differences between the rotamers become smaller with increasing nuclear charge of the heteroatom, see Table 5, with the two other rotamers being quasi degenerate within the accuracy of the applied calculations. Therefore, we used the all anti rotamer (Figure 1) as the reference to calculate the inversion barriers for the divinyl compounds. It is reasonable to expect that the energy differences for the various rotamers of the diethyl compounds are even lower than for the divinyl compounds and their influence on the inversion barriers can be neglected.

Inversion Barriers. Table 6 shows that the inversion barrier (ΔE_a; not corrected for zero-point vibrational energies) increases from nitrogen to bismuth for all series of compounds. As mentioned before, the angle β which describes the deviation from planarity about the pnicogen atom (see eq 1) also increases from nitrogen to bismuth. We found empirically that the correlation of β with the calculated inversion barrier can be described by an exponential function of the form

$$\Delta E_a = a\{e^{-b(360^\circ-(\alpha CXC'+\alpha CXH+\alpha C'XH)} - 1\} \qquad (2)$$

with ΔE_a in kJ mol^{-1} and all angles in degrees. The agreement between the calculated data and the fit is demonstrated in Figure 6 for the MP2 results. R^2 values for the obtained fits vary between 0.979 and 0.997 and the parameters a and b are as follows at the B3LYP/MP2 level: a = 5.576/3.593, b = 0.039/0.042 for HMC_4H_4; a = 3.074/4.255, b = 0.055/0.050 for $HM(C_2H_3)_2$; a = 21.586/23.054, b =0.032/0.030 for $HM(C_2H_5)_2$.

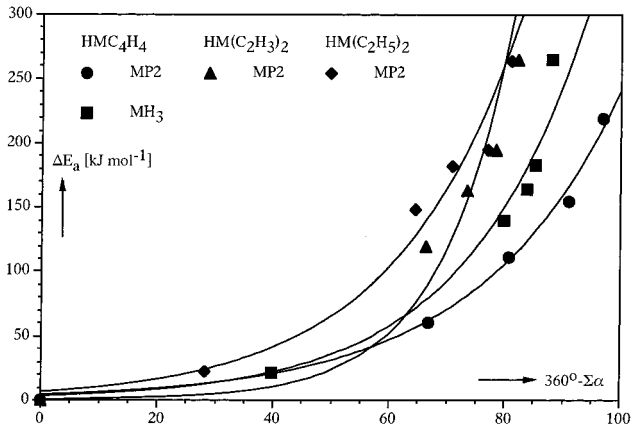

Figure 6. MP2 inversion barriers ΔE_a against the angle $\beta = 360^\circ - \Sigma\alpha$ as defined in eq 1 for MH_3, HMC_4H_4, $HM(C_2H_3)_2$, and $HM(C_2H_5)_2$ (M = N, P, As, Sb, and Bi).

For the diethyl compounds, we find quite similar inversion barriers as for NH_3 and PH_3. Because the ethyl group has a similar, only slightly higher electronegativity than hydrogen, this result is not surprising. On the basis of the electronegativity, one would also expect a slightly higher barrier for the divinyl and cyclic compounds, because the electronegativity of the carbon atom increases with the s-character, i.e., sp^2 versus sp^3 hybridization. However, the inversion barrier for most divinyl compounds is lower than that for their corresponding diethyl compounds, and the ring systems show the smallest inversion barriers. Particularly large effects are observed for the inversion barriers of the nitrogen and phosphorus containing molecules and for the ring systems. Differences between the vinyl and the alkyl derivatives are less pronounced and only marginal for the heavier elements As to Bi. As indicated by the Julg index, the transition states for the cyclic compounds possess significant aromatic character that leads to their stabilization. The divinyl compounds also profit from a conjugated π-bond system in the planar transition state, in particular for the lighter homologues.

Comparing the HF with the MP2 inversion barriers we observe that electron correlation effects reduce the inversion barrier, sometimes significantly so. This is in contrast to Freed's assumption that correlation can be neglected for classical rotation and inversion processes,[35] but in agreement with similarly large correlation effects predicted earlier by Nyulászi for phosphole.[9] Correlation effects are slightly more pronounced for the heavier elements and their contribution to the inversion barrier is particularly large for the ring system. We find the overall trend in correlation contributions to be $\Delta_C E_a(HMC_4H_4) > \Delta_C E_a(HM(C_2H_3)_2) > \Delta_C E_a(HM(C_2H_5)_2) > \Delta_C E_a(MH_3)$.[3] It is well-known that *Hartree−Fock* calculations give only an incomplete description of aromatic stabilization. Because the ring systems exhibit significant aromatic character in their planar transition state their inversion barrier is most reduced by correlation effects. Similarly, the divinyl compounds experience a stronger stabilization than the diethyl counterparts due to conjugation in the planar transition state.

Relation to HOMO−LUMO Energy Differences. For a classical inversion process of pyramidal MX_3 molecules, the distortion from the ideal high symmetry state of D_{3h} symmetry to C_{3v} can be understood as a second-order Jahn−Teller (SOJT) distortion. The minimum energy inversion path q is of C_{3v} symmetry and can be used to model the inversion process. The strength of the SOJT distortion is often discussed in terms of the HOMO−LUMO gap of the appropriate symmetries. To illustrate this we apply a one-dimensional Taylor expansion

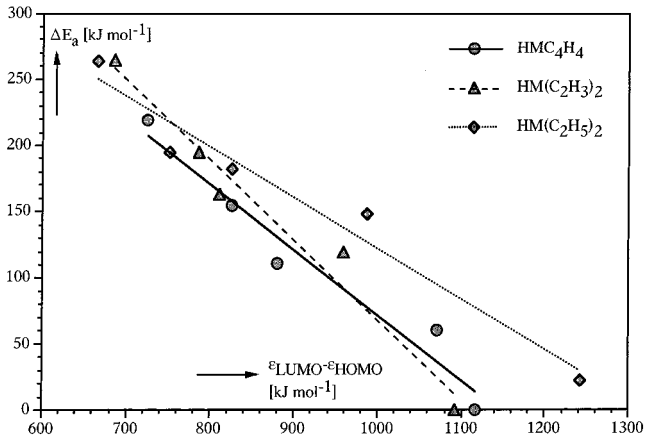

Figure 7. Inversions barriers ΔE_a versus the HOMO−LUMO gaps $\Delta\epsilon$.

around the high symmetry point and use perturbation theory up to second order[4]

$$E(q) = E_0 + \langle\psi_0|\partial\mathbf{H}/\partial q|\psi_0\rangle q + \left\{\frac{1}{2}\langle\psi_0|\partial^2\mathbf{H}/\partial q^2|\psi_0\rangle - \sum_n \frac{|\langle\psi_n|\partial\mathbf{H}/\partial q|\psi_0\rangle|^2}{E_n - E_0}\right\}q^2 + \ldots \quad (3)$$

with the excited state ψ_n, the ground state ψ_0, and the corresponding energies E_n and E_0 at the chosen high symmetry point (planar C_2MH arrangement). The second term describes the first-order Jahn−Teller (FOJT) term (if nonzero the system must distort) and the last term in eq 3 gives the SOJT term. The denominator $E_n - E_0$ in the last term can be approximated by the corresponding orbital energy differences according to Koopmans' theorem, $\Delta\epsilon = \epsilon_n - \epsilon_0$, for all $\langle\psi_n|\partial\mathbf{H}/\partial q|\psi_0\rangle \neq 0$, which in most cases is related to the HOMO−LUMO gap. The smaller the HOMO−LUMO gap, the larger the distortion and therefore the inversion barriers. This correlation is shown in Figure 7, based on the *Hartree−Fock* orbital energies. The inversion barriers ΔE_a decreases from bismuth to nitrogen with increasing HOMO−LUMO gap for all classes of compounds. The similar character of frontier orbitals in MH_3 and the $HM(C_4H_4)$ systems is depicted in the orbital plot in Figure 8 for the HOMOs of PH_3 and phosphole. The HOMO changes from a pure p-orbital for the D_{3h} structure of PH_3 into a sp^3-orbital for the minimum C_{3v} structure and we observe a similar change for phosphole.

Nonplanar Pyrrole Derivatives? The inversion barriers in Group 15 compounds of the form MX_3 increases with the electronegativity of the ligands X for a classical inversion, i.e., an inversion following along a C_{3v} path via a D_{3h} structure.[4] This concept can be generalized for other pnicogen compounds. So are phosphole derivatives, bearing the very electropositive $-BH_2$ group predicted to have almost no inversion barrier.[9,10] The question therefore arises if the introduction of electronegative ligands can lead to a nonplanar minimum structure for pyrrole, as predicted before for *p*-pyridone.[36] We therefore studied the tetrafluorinated cyclic compounds $HM(C_4F_4)$ together with perfluorinated pyrrole at the B3LYP level. The structures are shown in Figure 9 and relevant data are collected in Table 7.

For tetrafluoropyrrole a nonplanar minimum structure is indeed obtained, but the inversion barrier is very small and lies with only 0.5 kJ mol^{-1} outside the accuracy of our calculations. Fluorine substitution at the carbon atoms reduces the aromatic character of the ring sufficiently to cause a distortion from C_{2v} to C_s. The Julg index decreases from 0.940 for pyrrole to 0.883

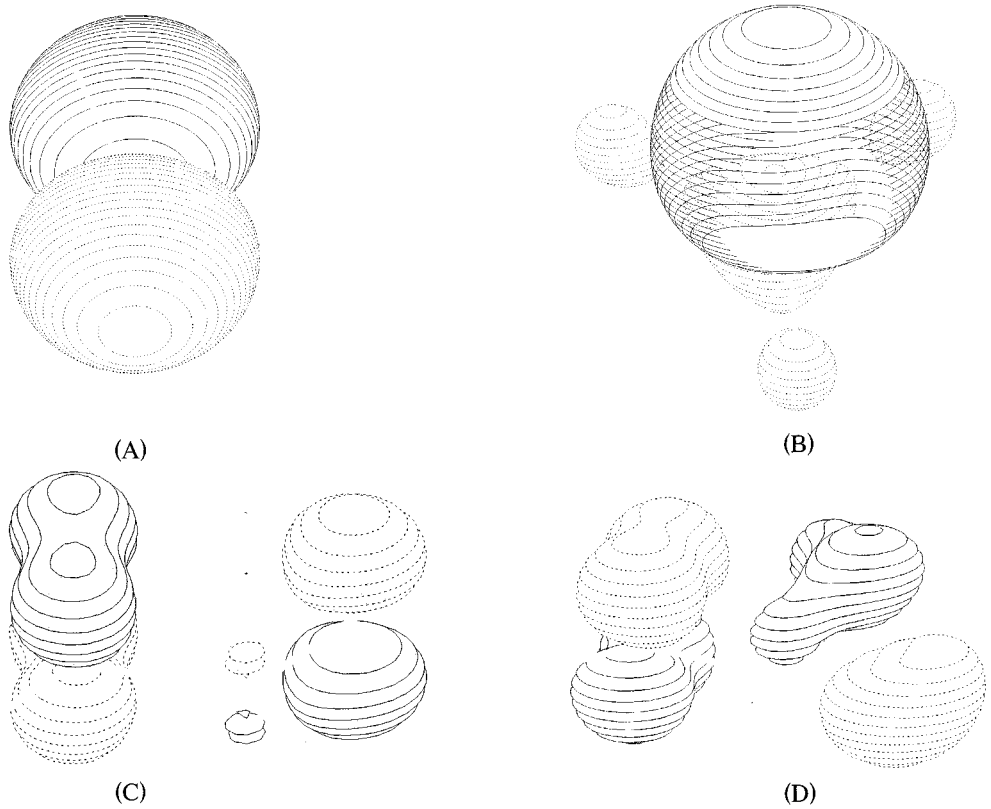

Figure 8. HOMOs of PH_3 (A) and (B) and phosphole (C) and (D) in the planar (A) and (C) and minimum nonplanar arrangement (B) and (D). The phosphorus atom in phosphole is on the right-hand side of the ring structure. Also seen is the C2═C2′ π-orbital on the left-hand side of the ring structure.

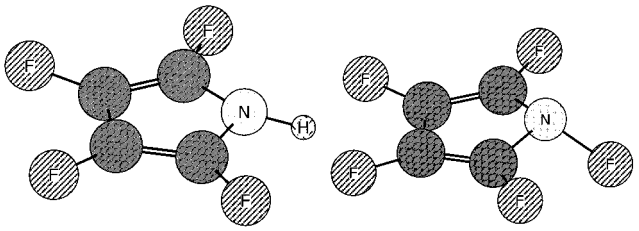

Figure 9. Optimized B3LYP structures of tetrafluoropyrrole and perfluoropyrrole.

TABLE 7: Selected Optimized Molecular Structure Parameters (in Å and degrees) and Inversions Barriers ΔE_a in kJ/mol^{-1} for the Minimum (C_{2v}) and Transition Structures (C_s) of HMC_4F_4 (M = N, P, As, Sb, and Bi), FNC_4H_4, and C_4F_5N at the B3LYP Level of Theory[a]

	sym	r_{M-C1}	r_{M-L}	r_{C1-C2}	$r_{C2-C2'}$	$\alpha_{C1-M-C1'}$	$360-\Sigma\alpha$	ΔE_a
					HMC_4F_4			
N	C_s	1.378	1.012	1.358	1.433	107.7	6.3	0.52
	C_{2v}	1.372	1.009	1.362	1.429	108.4	0	
P	C_s	1.836	1.425	1.338	1.462	87.8	77.1	135.4
	C_{2v}	1.748	1.392	1.370	1.425	95.5	0	
As	C_s	1.965	1.531	1.334	1.466	83.8	86.6	191.6
	C_{2v}	1.859	1.475	1.364	1.429	91.6	0	
Sb	C_s	2.165	1.722	1.334	1.471	78.6	94.1	231.2
	C_{2v}	2.065	1.653	1.358	1.439	85.0	0	
Bi	C_s	2.257	1.814	1.333	1.473	76.5	98.0	299.7
	C_{2v}	2.149	1.728	1.356	1.438	82.6	0	
					FNC_4H_4			
	C_{2v}	1.360	1.375	1.379	1.418	113.7	0	
					C_4F_5N			
	C_s	1.407	1.419	1.341	1.461	107.2	28.2	25.5
	C_{2v}	1.373	1.359	1.369	1.423	111.2	0	

[a] See Figures 2 and 6 for details.

for the planar structure of tetrafluoropyrrole. However, it is doubtful that this nonplanar structure could be observed in either solution or the gas phase, for example by electron gas diffraction since the system will most likely adopt a dynamic structure. For the other cyclic pnicogen compounds fluorination of the carbon atoms leads to a substantial increase in the inversion barrier between 50 and 70 kJ mol^{-1} (Table 7). A fifth fluorine substituent on the nitrogen increases the inversion barrier significantly and we calculate a value of 25.5 kJ mol^{-1} for perfluoropyrrole. Note however, that fluorine substitution at the nitrogen atom alone is not sufficient to break the planarity of the ring system. Our calculations predict a C_{2v} minimum for 1-*N*-fluoropyrrole (see Table 7). The inversion barrier for perfluoropyrrole is comparable to that of ammonia but the large masses of the carbon atoms around nitrogen should prohibit any tunneling effects of perfluoropyrrole at low temperatures. Therefore, the nonplanar minimum structure should be observable by spectroscopic methods, and it would be interesting to synthesize this compound.

4. Conclusion

The study of the Group 15 analogues of pyrrole, compounds HMC_4H_4, $HM(C_2H_3)_2$, and $HM(C_2H_5)_2$ (M = N, P, As, Sb, and Bi), shows that inversion barriers increase from N to Bi and from the ring system to the vinyl and finally the alkyl derivatives. This increase in the inversion barrier nicely correlates with a decrease in the HOMO−LUMO gap as expected from a second-order Jahn−Teller distortion in a classical inversion process. π-conjugation in the minimum decreases with increasing nuclear charge of the heteroatom and from the cyclic to the diethyl compounds. Only pyrrole and divinylamine exhibit a planar geometry about the heteroatom. However, nonplanar pyrrole derivatives can be obtained by fluorination of the ring system, or even better by fluorination of all five atoms in the heterocycle. Deviation from planarity in pyrrole derivatives has not been yet observed and the synthesis of perfluoropyrrole is therefore of interest.

Acknowledgment. The Auckland University Research Committee and the Marsden Fund administered by the Royal Society of New Zealand supported this work.

References and Notes

(1) Dennison, D. M.; Hardy, J. D. *Phys. Rev.* **1932**, *39*, 938.
(2) Dommen, J.; Caminati, W.; Hollenstein, H.; Ha, T.-K.; Meyer, R.; Bauder, A. *J. Mol. Spectrosc.* **1996**, *180*, 369.
(3) Schwerdtfeger, P.; Laakkonen, L.; Pyykkö, P. *J. Chem. Phys.* **1992**, *96*, 6807.
(4) See for example: (a) Marynick, D. S.; Dixon, D. A. *J. Phys. Chem.* **1982**, *86*, 914. (b) Dixon, D. A.; Arduengo, A. J., III *J. Am. Chem. Soc.* **1987**, *109*, 338. (c) Balasubramanian, K.; Chung, Y. S.; Glaunsinger, W. S. *J. Chem. Phys.* **1993**, *98*, 8859. (d) Creve, S.; Nguyen, M. T. *J. Phys. Chem. A* **1998**, *102*, 6549.
(5) Schwerdtfeger, P.; Hunt, P. *Adv. Mol. Struct. Res.* **1999**, *5*, 223.
(6) For reviews on phospholes, see: (a) Mathey, F. *Chem. Rev.* **1988**, *88*, 429. (b) Mathey, F. *J. Organomet. Chem.* **1990**, *400*, 149. (c) Quin, L. D. *Compr. Heterocycl. Chem. II* **1996**, *2*, 757.
(7) Rauk, A.; Allen, L. C.; Mislow, K. *Angew. Chem., Int. Ed. Engl.* **1970**, *9*, 400.
(8) Elschenbroich, C.; Salzer, A. *Organometallics, A Concise Introduction*; VCH: Weinheim, 1992.
(9) Nyulászi, L. *J. Phys. Chem.* **1995**, *99*, 586.
(10) Delaere, D.; Dransfeld, A.; Nguyen, M. T.; Vanquickenborne, L. G. *J. Org. Chem.* **2000**, *65*, 2631.
(11) (a) Nyulászi, L. *Inorg. Chem.* **1996**, *35*, 4690. (b) Glukhovtsev, M. N.; Dransfeld, A.; Schleyer, P. v. R. *J. Phys. Chem.* **1996**, *100*, 13 447. (c) Dransfeld, A.; Nyulászi, L.; Schleyer, P. v. R. *Inorg. Chem.* **1998**, *37*, 4413.
(12) (a) Dixon, D. A.; Arduengo, A. J.; Fukunaga, T. *J. Am. Chem. Soc.* **1986**, *108*, 2461. (b) Arduengo, A. J.; Dixon, D. A.; Roe, D. C. *J. Am. Chem. Soc.* **1986**, *108*, 6821.
(13) For example: (a) Baldrigde, K. K.; Gordon, M. S. *J. Am. Chem. Soc.* **1988**, *110*, 4204. (b) Chesnut, D. B.; Quin, L. D. *J. Am. Chem. Soc.* **1994**, *116*, 9638. (c) Chesnut, D. B. *J. Comput. Chem.* **1995**, *16*, 1227. (d) Schleyer, P. v. R.; Freeman, P. K.; Jiao, H.; Goldfuss, B. *Angew. Chem., Int. Ed. Engl.* **1995**, *34*, 337. (e) Schleyer, P. v. R.; Maerker, C.; Dransfeld, A.; Jiao, H.; van Eikema Hommes, N. J. R. *J. Am. Chem. Soc.* **1996**, *118*, 6317. (f) Chesnut, D. B.; Bartolotti, L. J. *Chem. Phys.* **2000**, *257*, 175.
(14) For example: (a) Bachrach, S. M. *J. Org. Chem.* **1993**, *58*, 5414. (b) Hinchcliffe, A.; Soscun, M. H. J. *Theochem. (J. Mol. Struct.)* **1995**, *331*, 109. (c) Salzner, U.; Bachrach, S. M.; Mulhearn, D. C. *J. Comput. Chem.* **1997**, *18*, 198. (d) Salzner, U.; Bachrach, S. M. *J. Organomet. Chem.* **1997**, *15*, 529.
(15) Caster, K. C. *Compr. Heterocycl. Chem. II* **1996**, *2*, 857.
(16) (a) Wilson, A.; van Mourik, T.; Dunning, T. H., Jr. *J. Mol. Struct. (THEOCHEM)* **1996**, *388*, 339. (b) Woon, D. E.; Dunning, T. H., Jr. *J. Chem. Phys.* **1993**, *98*, 1358.
(17) Frisch, M. J.; Trucks, G. W.; Schlegel, H. B.; Scuseria, G. E.; Robb, M. A.; Cheeseman, J. R.; Zakrzewski, V. G.; Montgomery, J. A.; Stratman, R. E.; Burant, J. C.; Dapprich, S.; Millam, J. M.; Daniels, A. D.; Kudin, K. N.; Strain, M. C.; Farkas, O.; Tomasi, J.; Barone, V.; Cossi, M.; Cammi, R.; Mennucci, B.; Pomelli, C.; Adamo, C.; Clifford, S.; Ochterski, J.; Petersson, G. A.; Ayala, P. Y.; Cui, Q.; Morokuma, K.; Malick, D. K.; Rabuck, A. D.; Raghavachari, K.; Foresman, J. B.; Cioslowski, J.; Ortiz, J. V.; Stefanov, B. B.; Liu, G.; Liashenko, A.; Piskorz, P.; Komaromi, I.; Gomperts, R.; Martin, R. L.; Fox, D. J.; Keith, T.; Al-Laham, M. A.; Peng, C. Y.; Nanayakkara, A.; Gonzalez, C.; Challacombe, M.; Gill, P. M. W.; Johnson, B. G.; Chen, W.; Wong, M. W.; Andres, J. L.; Head-Gordon, M.; Replogle, E. S.; Pople, J. A. *Gaussian 98*, Revision A.1; Gaussian, Inc.: Pittsburgh, PA, 1998.
(18) Becke, A. D. *J. Chem. Phys.* **1993**, *98*, 5648.
(19) Lee, C.; Yang, W.; Parr, R. G. *Phys. Rev. B* **1988**, *37*, 785.
(20) Stoll, H.; Dolg, M.; Preuss, H. *Pseudopotential Parameters and Basis Sets*, Internal Report; Universität Stuttgart: Stuttgart, 1997.
(21) Halkier, A.; Taylor, P. R. *Chem. Phys. Lett.* **1998**, *285*, 133.
(22) Császár, A. G.; Allen, W. D.; Schaefer, H. F., III *J. Chem. Phys.* **1998**, *108*, 9751.
(23) Swalen, J. D.; Ibers, J. A. *J. Chem. Phys.* **1962**, *36*, 1914.

(24) Klopper, W.; Samson, C. C. M.; Tarczay, G.; Császár, A. G. *J. Comput. Chem.* **2001**, *22*, 1306.
(25) Handy, N. C.; Carter, S.; Colwell, S. M. *Mol. Phys.* **1999**, *96*, 477.
(26) Spirko, V.; Kraemer, W. P. *J. Mol. Spectrosc.* **1989**, *133*, 331, and references therein.
(27) Maessen, B.; Bopp, P.; McLaughlin, D. R.; Wolfsberg, M. *Z. Naturforsch. A* **1984**, *39*, 1005.
(28) Nakamoto, K. *Infrared and Raman Spectra of Inorganic and Coordination Compounds, Part A: Theory and Applications in Inorganic Chemistry*; Wiley: New York, 1997.
(29) Nygaard, L.; Nielsen, J. T.; Kirchheiner, J.; Maltesen, G.; Rastrup-Andersen, J.; Sørensen, G. O. *J. Mol. Struct.* **1969**, *3*, 491.
(30) Takeuchi, H.; Kojima, T.; Egawa, T.; Konaka, S. *J. Phys. Chem.* **1992**, *96*, 4389.
(31) (a) Guillemin, J.-C.; Lassalle, L. *Organometallics* **1994**, *13*, 1525. (b) Lassalle, L.; Legoupy, S.; Guillemin, J.-C. *Organometallics* **1996**, *15*, 3466.
(32) Using the crystal structure of 1-benzylphosphole for comparison, see: Coggon, P.; Engel, J. F.; McPhail, A. T.; Quin, L. D. *J. Am. Chem. Soc.* **1970**, *92*, 5779.
(33) Schwerdtfeger, P.; Boyd, P. D. W.; Fischer, T.; Hunt, P.; Liddell, M. *J. Am. Chem. Soc.* **1994**, *116*, 9620.
(34) Julg, A.; Francois, P. *Theor. Chim. Acta* **1967**, *8*, 249.
(35) Freed, K. F. *Chem. Phys. Lett.* **1968**, *2*, 255.
(36) Hunt, P. A.; Schwerdtfeger, P. *J. Org. Chem.* **1997**, *62*, 8063.